

Effect of Patch Size on Fine-Tuning Vision Transformers in Two-Dimensional and Three-Dimensional Medical Image Classification

Massoud Dehghan^a, Ramona Woitek^a, Amirreza Mahbod^{a,1}

^a*Research Center for Medical Image Analysis and Artificial Intelligence, Department of Medicine, Faculty of Medicine and Dentistry, Danube Private University, Krems an der Donau, 3500, Austria*

Abstract

Vision Transformers (ViTs) and their variants have become state-of-the-art in many computer vision tasks and are widely used as backbones in large-scale vision and vision-language foundation models. While substantial research has focused on architectural improvements, the impact of patch size, a crucial initial design choice in ViTs, remains underexplored, particularly in medical domains where both two-dimensional (2D) and three-dimensional (3D) imaging modalities exist.

In this study, using 12 medical imaging datasets from various imaging modalities (including seven 2D and five 3D datasets), we conduct a thorough evaluation of how different patch sizes affect ViT classification performance. Using a single graphical processing unit (GPU) and a range of patch sizes (1, 2, 4, 7, 14, 28), we fine-tune ViT models and observe consistent improvements in classification performance with smaller patch sizes (1, 2, and 4), which achieve the best results across nearly all datasets. More specifically, our results indicate improvements in balanced accuracy of up to 12.78% for 2D datasets (patch size 2 vs. 28) and up to 23.78% for 3D datasets (patch size 1 vs. 14), at the cost of increased computational expense. Moreover, by applying a straightforward ensemble strategy that fuses the predictions of the models trained with patch sizes 1, 2, and 4, we demonstrate a further boost in per-

Email addresses: massoud.dehghan@dp-uni.ac.at (Massoud Dehghan), ramona.woitek@dp-uni.ac.at (Ramona Woitek), amirreza.mahbod@dp-uni.ac.at (Amirreza Mahbod)

¹Corresponding Author

formance in most cases, especially for the 2D datasets. Our implementation is publicly available on GitHub: <https://github.com/HealMaDe/MedViT>

Keywords: Vision Transformer, Patch Size, Medical image classification, Deep Learning, Medical image Analysis

1. Introduction

The broad range of medical imaging modalities, such as magnetic resonance imaging (MRI), computed tomography (CT), dermatoscopy, X-ray, and ultrasound, which forms the backbone of modern medicine, has created a noticeable demand for automated analysis systems for downstream tasks such as detection, segmentation, and classification [1, 2]. These systems can help reduce diagnostic errors made by medical experts, as they can process large volumes of data efficiently and learn patterns present in the data [3, 4]. Among the various tasks defined in medical computer vision, image classification is one of the fundamental tasks, where the aim is to assign a label to an entire image, for example, benign versus malignant [5].

While many automatic methods have been proposed for medical image classification, deep learning techniques, particularly convolutional neural networks (CNNs), have shown highly promising results over the past decade compared to traditional image processing or classical machine learning (ML) approaches. Popular CNN-based models such as ResNet [6], DenseNet [7], and EfficientNet (V1 and V2) [8, 9] and ensemble CNNs [10] have set new benchmarks in a wide range of medical and non-medical image classification tasks [11, 6, 12, 13]. These models learn hierarchical image features automatically without the need for manual feature extraction, which is one of their key advantages over classical ML methods that rely on potentially suboptimal hand-crafted features [14].

Convolutional kernels are effective feature extractors within their local receptive fields, but the inherent locality bias of CNNs limits their capacity to capture long-range dependencies in images. As a newer alternative to traditional convolutional architectures, vision transformers (ViTs) [15] rely on self-attention mechanisms that directly model global relationships between image patches, enabling a more flexible and expressive representation of contextual information [16, 17]. ViTs were originally inspired by transformer architectures [18] developed for natural language processing, and were adapted to vision tasks such as image classification through techniques in-

cluding patch embedding and positional encoding [15]. Several studies have shown that ViT-based architectures outperform CNNs in various medical imaging tasks, demonstrating improved generalization and robustness across modalities [19, 20, 21]. Due to their excellent performance, many large-scale medical and non-medical foundation models, such as MedCLIP [22], BioMedCLIP [23], UNI [24] and OpenCLIP [25], use ViTs as their backbone architecture, and these models have been widely adopted for downstream clinical and computational applications [26, 27, 28].

As stated in [15], in a ViT, an input image is first split into fixed-size patches. Each patch is then flattened and transformed into patch embeddings. A learnable class token is added to the start of the sequence, and positional embeddings are included to keep spatial information. The sequence goes through several transformer encoder layers, which include multi-head self-attention and feed-forward networks. This setup enables interaction of global features among patches. Finally, the output of the final ViT encoder block is connected to a classification head (e.g., a multi-layer perceptron) to predict the image label.

Since the introduction of the first ViT models, several novel and modified approaches, such as Swin Transformers (V1 and V2) [29, 30], and hybrid CNN-Transformer architectures [31, 32, 33] have been proposed to boost performance in visual recognition tasks. However, one fundamental component of ViT pipelines that is rarely discussed in the literature is the patching strategy used to tokenize the input images. Most ViT-based methods rely on a fixed patch size (commonly 14×14 or 16×16), even though patch size directly determines the number of tokens and, therefore, the model’s ability to capture fine-grained spatial information. In this study, our goal is to specifically examine the impact of different patch sizes on the overall performance of ViT for medical image classification. To the best of our knowledge, very few studies have explored ViTs from this perspective, particularly in the context of medical imaging, where both 2D and 3D datasets differ structurally from natural images.

Than et al. performed a preliminary evaluation of ViTs for classifying COVID-19 and lung diseases. They used various patch sizes, ranging from 16×16 to 256×256 . Their findings indicated that choosing the right patch size can greatly affect classification performance, with larger patches leading to a noticeable drop in accuracy. However, they did not explore what happened to the performance if the size of the patches decreased [34]. In another study carried out by Liu et al., eliminating unnecessary input patches was

examined to reduce computational cost with maintaining performance on high-resolution medical image classification tasks, although the systematic effect of patch sizes alone was not tested [35]. Similarly, without considering the effect of various patch sizes, Halder et al. showed ViT models can achieve state-of-the-art performance across diverse 2D biomedical imaging tasks using the MedMNIST V2 collection [36, 37]. Additionally, Beyer et al. proposed FlexiViT, which is based on randomized patch sizes and adaptive positional embedding, and achieved better results compared to fixed patch sizes. However, the impact of specific patch-size choices was not discussed in their work [38]. Finally, two research efforts closely related to our work investigated the effect of reducing ViT patch sizes on performance. Nguyen et al. showed that in a supervised learning setting, ViTs can benefit from smaller patch sizes while keeping the input image size fixed [39]. Similarly, Wang et al. reported consistent improvements in performance as patch sizes were reduced, revealing a scaling law in patchification in which accuracy continues to increase as patch size decreases [40]. However, both studies focused solely on 2D natural images and did not consider either 2D or 3D medical images. Moreover, the models in these studies were trained from scratch, which is often not feasible for small-scale medical imaging datasets, where fine-tuning is generally the preferred approach [41].

In summary, there remains a clear gap in the literature regarding the systematic investigation of patch-size effects on medical image data. Most existing ViT-based studies have been developed and evaluated using natural image datasets rather than medical images. In addition, these models are often trained from scratch instead of being fine-tuned on domain-specific data. Current research also focuses almost entirely on 2D images, even though many medical imaging modalities, such as MRI and CT, are inherently 3D and require volumetric modeling for accurate diagnosis. Moreover, training of large-scale ViT models in previous studies has frequently relied on multiple high-end graphical processing units (GPU) or tensor processing units (TPU) clusters and substantial computational resources (for example, 50,000 A100 GPU hours in [40] or 10,000 TPU-core days in [42]), creating a significant computational barrier for many research groups.

In contrast, our study tackles all these limitations. We provide the first complete evaluation of how progressively smaller patch sizes affect ViT-based classification performance in both 2D and 3D medical imaging modalities. Importantly, we show that detailed patch-size analysis is possible on a single, modest GPU, as long as the appropriate dataset is used. These find-

ings emphasize the practicality of conducting detailed tokenization studies in real-world research settings and offer new insights into the best patch-size selection for medical image analysis.

The main contributions of this study can be summarized as follows:

- We perform a thorough evaluation of the impact of patch size on the classification performance of ViTs.
- We focus on fine-tuning ViTs, a common approach in the medical domain, and include both 2D and 3D medical imaging datasets using a single GPU setup in our experiments.
- Our implementation is publicly available, which supports transparency and reproducibility of our results.

In the rest of the paper, we explain our methodology and implementation setup in Section 2, report and discuss the results in Section 3, and conclude the work in Section 4.

2. Methodology

In ViTs, the computational complexity of the multi-head self-attention mechanism grows quadratically with the number of input tokens (T). So, the self-attention cost per layer is proportional to $O(T^2.d)$, where d is the embedding dimension [43].

To analyze how patch size affects computational cost (C), we compare a standard patch size of $p \times p$ with a smaller patch size of $\frac{p}{N} \times \frac{p}{N}$. For a 2D image of size $H \times W$, reducing the patch size raises the number of patches (tokens) from $T_1 = \frac{HW}{p^2}$ to $T_2 = N^2 T_1$, which shows a growth factor of N^2 . Since the self-attention operation scales with the square of the number of tokens, the attention cost per layer goes up from $C_1 \propto T_1^2$ to $C_2 \propto (N^2 T_1)^2 = N^4 T_1^2$. As a result, the self-attention computation cost increases by a factor of N^4 . Extending this reasoning to 3D inputs with volume $H \times W \times D$ and 3D patches of size $p \times p \times p$, reducing the patch size to $\frac{p}{N}$ in each dimension increases the number of tokens from $T_1 = \frac{HWD}{p^3}$ to $T_2 = N^3 T_1$, a growth factor of N^3 . Consequently, the self-attention cost rises from $C_1 \propto T_1^2$ to $C_2 \propto (N^3 T_1)^2 = N^6 T_1^2$. Therefore, in 3D ViTs, decreasing the patch size by a factor of N in each dimension increases the self-attention computation cost by N^6 , demonstrating the severe scaling challenges introduced by finer 3D

tokenization. For example, halving the patch size (from p to $\frac{p}{2}$) multiplies the self-attention cost by $16\times$ in 2D, and by $64\times$ in 3D due to cubic token growth.

This steep increase in computational cost explains why smaller patches, although potentially beneficial for fine-grained feature extraction (as shown in the results section), have not been thoroughly investigated in the literature. To ensure that our study remains feasible on a single GPU setup, we carefully selected a variety of datasets that contain small-sized images and volumes (28×28 for 2D datasets and $28\times 28\times 28$ for 3D datasets).

2.1. Dataset

We use a subset of the MedMNIST V2 collection [37], which provides a variety of biomedical image-classification datasets: seven 2D subsets and five 3D subsets from various imaging modalities, as summarized in Table 1. Visual examples of the selected datasets are shown in Figure 1. Although the MedMNIST V2 collection provides datasets in various resolutions (up to 224 for 2D datasets and up to 64 for 3D datasets), we use the smallest available size, namely 28×28 for 2D datasets and $28\times 28\times 28$ for 3D datasets, to ensure that all experiments can be run in a single GPU setup.

We explicitly choose the MedMNIST V2 collection because it contains images from a wide range of imaging modalities in both 2D and 3D formats, which allows us to perform a comprehensive analysis across diverse types of medical images. The selected datasets include both binary and multi-class classification tasks, as indicated in Table 1.

2.2. Preprocessing

From the seven 2D datasets, five are already provided in RGB format, while two (BreastMNIST and PneumoniaMNIST) are grayscale. For the grayscale datasets, we replicate the single channel three times to create an RGB-like three-channel representation, ensuring compatibility with models that require RGB inputs. Data augmentation is applied during training to artificially increase the dataset size, including random resized cropping, horizontal flipping, rotation, and light color adjustments.

For the 3D datasets, the volumetric images ($28\times 28\times 28$) are first converted to tensors and then replicated across three channels ($28\times 28\times 28\times 3$) to meet the model input requirements. We also apply simple 3D spatial augmentations, such as random flipping and rotations, during training.

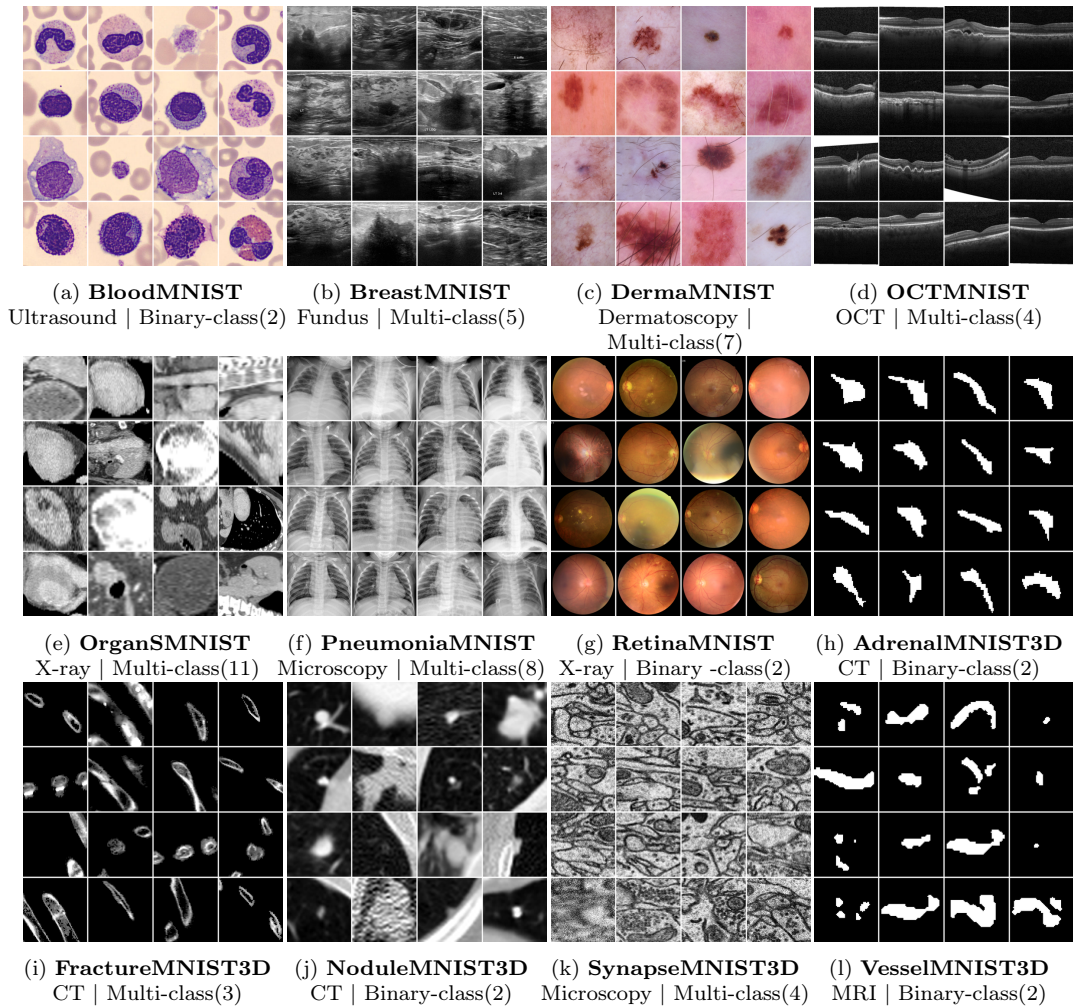


Figure 1: Overview of the 12 selected datasets from the MedMNIST V2 collection used in this study. Each sub-figure shows some representative example images along with the dataset name, imaging modality, and classification task. For the 3D datasets, the middle slices from random samples are shown.

Table 1: Summary of the selected datasets from MedMNIST V2 collection [37].

Dataset	Type	# train/val/test	classes	Modality
Breast	2D	546/78/156	2	Ultrasound
Retina	2D	1080/120/400	5	Fundus imaging
Blood	2D	11959/1712/3421	8	Microscopy
Derma	2D	7007/1003/2005	7	Dermatoscopy
OCT	2D	97477/10832/1000	4	Retinal OCT
OrganS	2D	13932/2452/8827	11	Abdominal CT
Pneumonia	2D	4708/524/624	2	X-ray
Adrenal	3D	1188/98/298	2	Abdominal CT
Fracture	3D	1027/103/240	3	Chest CT
Nodule	3D	1158/165/310	2	Chest CT
Synapse	3D	1230/177/352	2	Electron Microscopy
Vessel	3D	1335/191/382	2	Brain MRA

2.3. Fine-Tuning Pretrained ViT Models

ViTs are available in multiple scales, defined by the number of transformer layers, embedding dimension, and number of attention heads. These configurations result in several variants such as Tiny, Small, Base, Large, and Huge. For our experiments, we use the ViT-Small model, which includes 12 transformer layers, an embedding dimension of 384, and 6 attention heads, totaling approximately 22 million parameters. This configuration provides a strong balance between performance and computational efficiency. We use the ImageNet-pretrained weights [44], which allows for efficient transfer learning with limited medical data.

In 2D datasets, we replace the pretrained classification head with a new one that matches the number of classes in the target dataset, while keeping the transformer encoder trainable so it can adapt its learned features to the medical images.

In 3D datasets, we expand the pretrained weights using the weight inflation method introduced in [45]. We convert the original 2D patch embeddings into 3D kernels by repeating the weights along the depth axis. This method allows us to tokenize 3D images into non-overlapping 3D cubes. The number of tokens increases compared to the 2D case because of the extra depth dimension. To maintain geometric coherence, we reshape the pretrained 2D positional embeddings into a spatial grid and interpolate them to fit the 3D

token arrangement using trilinear interpolation.

2.4. Implementation Details and Prediction Fusion

Given that all input images are $28 \times 28 (\times 28)$, we evaluate models with patch sizes $P \in \{28, 14, 7, 4, 2, 1\}$. Using patch sizes that are factors of the input resolution allows the image to be divided into non-overlapping patches without needing padding or truncation. This setup keeps spatial integrity, prevents partial patches at the edges, and makes it easier to reshape the image grid into the sequence of tokens used by the Transformer. $P = 28$ represents a global image-level tokenization with a single 1×1 grid. $P = 14$ and $P = 7$ provide 2×2 and 4×4 grids for mid-level representation, respectively. Smaller patches ($P \leq 4$) capture fine local structures (see Figure 2 and Figure 3 for examples). This design gradually increases the number of tokens entered into the model and enables us to study how patch size affects both the model performance and computational cost.

Although this is not the main focus of this study, we also implement an ensembling strategy that fuses the predictions of the models trained with patch sizes of 1, 2, and 4 using straightforward averaging.

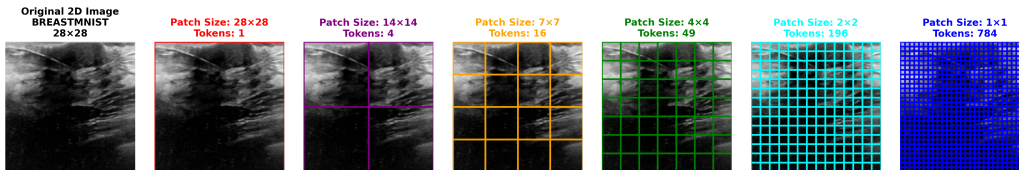


Figure 2: Example of splitting the image into patches with different sizes for 2D models.

All subset datasets follow standard splits into training, validation, and test partitions as provided by MedMNIST V2 [37]. This supports reproducible comparisons and consistent baselines across subsets. We created two training pipelines: one for 2D image classification and another for 3D volumetric data. They have the same experimental structure, optimization routine, and evaluation protocol, but differ only in input data dimensionality. Gradients are calculated through backpropagation, and the model parameters are updated using the AdamW optimizer [46] with a learning rate of 10^{-4} and a scheduler that halves the learning rate after every 25 epochs. The models are trained for 80 epochs using the cross-entropy loss function, and the best-performing checkpoint is selected based on the lowest validation loss. Model performance on the test set is evaluated using well-known

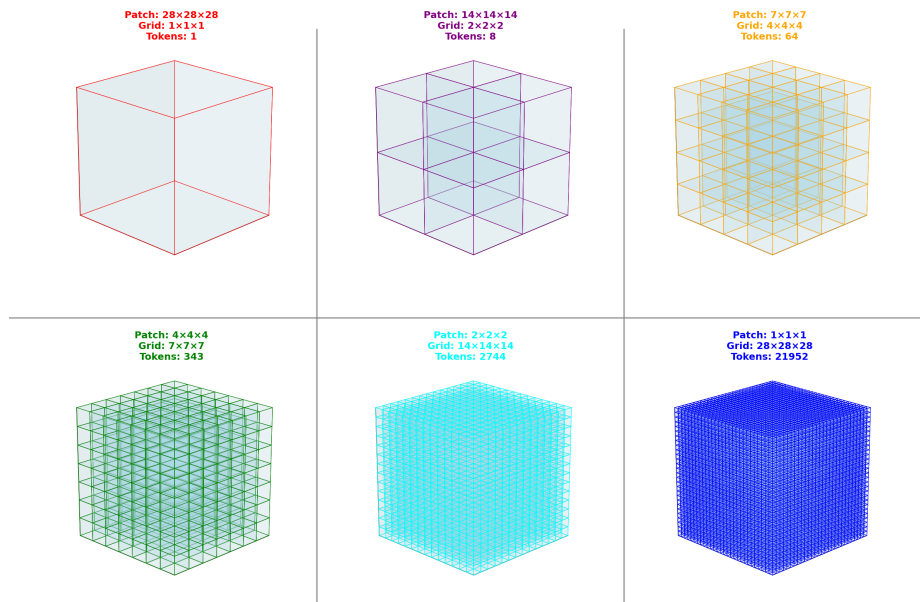


Figure 3: Example of splitting the image into patches with different sizes for 3D models.

metrics, including accuracy (Acc.), balanced accuracy (Bal. Acc.), and the area under the ROC curve (AUC). For AUC computation on multi-class datasets, a one-vs-rest approach is used. Each experiment is repeated three times to assess robustness, and results are reported as mean \pm standard deviation for all evaluation metrics. All experiments are conducted using a workstation with an AMD Ryzen 9 7950X CPU, 96 GB of RAM, and a single NVIDIA RTX 4090 GPU. Our implementation is publicly available on GitHub: <https://github.com/HealMaDe/MedViT>.

3. Results and Discussion

The experimental results for all 12 datasets are reported in Tables 2–13 based on Acc, Bal. Acc., AUC, and GFLOPs per test image for different patch sizes. We also report the ensemble results (prediction fusion of models trained with patch sizes of 1, 2, and 4) in the last row of each table. We organize our analysis into three groups: small-scale 2D datasets (Tables 2 and 3 for BreastMNIST and RetinaMNIST), medium- to large-scale 2D datasets (Tables 4 to 8 for BloodMNIST, DermaMNIST, OCTMNIST, OrganSMNIST and PneumoniaMNIST), and 3D datasets (Tables 9 to 13 for AdrenalM-

NIST3D, FractureMNIST3D, NoduleMNIST3D, SynapseMNIST3D and VesselMNIST3D). All reported results are averages over three runs along with the standard deviation.

3.1. Small-scale 2D Datasets

The results for the small-scale 2D datasets are shown in Tables 2 and 3. We present these results separately because fine-tuning on BreastMNIST and RetinaMNIST is affected by the limited number of training samples compared to the other 2D datasets (546 for BreastMNIST and 1080 for RetinaMNIST versus at least 4,708 training samples for the remaining 2D datasets). As the results indicate, performance varies more across patch sizes than in the larger datasets, suggesting that limited data may prevent the model from learning effective, patch-size-dependent features, leading to inconsistent performance patterns.

For BreastMNIST, the best performance is achieved with the proposed prediction fusion, but the effect of patch size on the performance is not clear. For RetinaMNIST, although the best Acc. and AUC are obtained with patch size 1, the best Bal. Acc. is obtained with patch size 28, again indicating an unclear pattern when fine-tuning on small-scale datasets. It is also worth noting that the performance differences across patch sizes for these two datasets are less pronounced than those observed in the other 2D datasets (refer to the results in the next section).

Table 2: Effect of patch size on classification performance for the **BreastMNIST** dataset. Acc.: Accuracy, Bal. Acc.: Balanced Accuracy, AUC: Area under the ROC curve, GFLOPs: Giga Floating-Point Operations.

Patch size	Acc. (%)	Bal. Acc. (%)	AUC (%)	GFLOPs
1	84.40 ± 0.98	77.05 ± 1.55	89.60 ± 2.02	16.71
2	85.04 ± 1.48	77.24 ± 0.38	90.07 ± 2.68	4.19
4	84.62 ± 1.93	76.94 ± 4.69	90.54 ± 0.90	1.06
7	85.26 ± 0.64	75.63 ± 0.44	87.29 ± 2.73	0.36
14	83.55 ± 1.34	76.21 ± 3.07	88.25 ± 1.75	0.11
28	83.76 ± 1.96	75.36 ± 2.59	84.11 ± 2.18	0.04
(1, 2, 4)	87.61 ± 0.80	80.74 ± 1.48	92.34 ± 0.61	21.96

Table 3: Effect of patch size on classification performance for the **RetinaMNIST** dataset. Acc.: Accuracy, Bal. Acc.: Balanced Accuracy, AUC: Area under the ROC curve, GFLOPs: Giga Floating-Point Operations.

Patch size	Acc. (%)	Bal. Acc. (%)	AUC (%)	GFLOPs
1	54.67 ± 1.63	36.71 ± 2.11	74.44 ± 0.57	16.71
2	51.08 ± 1.01	32.02 ± 2.67	71.78 ± 0.90	4.19
4	52.17 ± 0.76	34.51 ± 0.80	73.77 ± 1.94	1.06
7	53.25 ± 1.75	36.01 ± 0.51	73.68 ± 1.33	0.36
14	53.33 ± 2.32	35.58 ± 2.83	72.63 ± 1.72	0.11
28	54.08 ± 0.72	36.99 ± 0.50	72.73 ± 0.79	0.04
(1, 2, 4)	53.00 ± 0.71	34.71 ± 1.00	74.02 ± 0.50	21.96

3.2. Medium- to large-scale 2D Datasets

As the results in Tables 4 to 8 show, for the medium- and large-scale 2D datasets (with training set sizes ranging from 4,708 to 97,477), including BloodMNIST, DermaMNIST, OCTMNIST, OrganMNIST, and PneumoniaMNIST, the impact of patch size becomes clearer and more consistent. In nearly all datasets, reducing the patch size improves classification performance. More specifically, the best performances are achieved with patch sizes of 1, 2, or 4, whereas the worst performances are consistently obtained with patch size 28. This suggests that finer spatial tokenization enables ViTs to capture local shapes and textures more effectively.

Among the small patch sizes (1, 2, and 4), patch size 2 achieves the best overall performance and patch size 28 achieves the worst overall performance across all datasets (average Acc., Bal. Acc., and AUC of 89.74%, 79.73% , and 97.84% for patch size 2 versus 84.05%, 70.91%, and 96.23% for patch size 28). A detailed comparison between patch sizes 2 and 28 is provided in the supplementary material (Table S1), where the largest performance differences in Acc. and Bal. Acc. are observed in the OrganMNIST dataset at 12.12% and 12.78%, respectively. Based on AUC, the largest difference is seen in BreastMNIST at 5.96%.

Furthermore, beyond the individual patch sizes, the ensemble results that combine predictions from models trained with patch sizes 1, 2, and 4 provide the best overall performance. This further supports the idea that integrating multi-scale tokens derived from smaller patches enhances classification performance.

Table 4: Effect of patch size on classification performance for the **BloodMNIST** dataset. Acc.: Accuracy, Bal. Acc.: Balanced Accuracy, AUC: Area under the ROC curve, GFLOPs: Giga Floating-Point Operations.

Patch size	Acc. (%)	Bal. Acc. (%)	AUC (%)	GFLOPs
1	96.50 ± 0.13	96.03 ± 0.12	99.82 ± 0.03	16.71
2	96.99 ± 0.28	96.56 ± 0.41	99.87 ± 0.02	4.19
4	96.62 ± 0.92	96.09 ± 1.31	99.85 ± 0.03	1.06
7	96.46 ± 0.26	95.95 ± 0.44	99.82 ± 0.02	0.36
14	94.96 ± 0.14	94.33 ± 0.41	99.67 ± 0.02	0.11
28	93.59 ± 0.46	92.36 ± 0.60	99.50 ± 0.05	0.04
(1, 2, 4)	97.46 ± 0.10	97.10 ± 0.25	99.90 ± 0.01	21.96

Table 5: Effect of patch size on classification performance for the **DermaMNIST** dataset. Acc.: Accuracy, Bal. Acc.: Balanced Accuracy, AUC: Area under the ROC curve, GFLOPs: Giga Floating-Point Operations.

Patch size	Acc. (%)	Bal. Acc. (%)	AUC (%)	GFLOPs
1	78.70 ± 0.64	56.16 ± 3.02	94.18 ± 0.20	16.71
2	78.12 ± 0.33	54.86 ± 3.75	94.16 ± 0.36	4.19
4	78.65 ± 0.99	56.64 ± 2.30	94.37 ± 0.67	1.06
7	77.18 ± 0.94	54.38 ± 1.90	93.95 ± 0.38	0.36
14	75.86 ± 0.09	48.76 ± 3.03	92.16 ± 0.41	0.11
28	73.76 ± 0.56	42.23 ± 6.01	90.63 ± 0.51	0.04
(1, 2, 4)	80.52 ± 0.70	59.32 ± 2.70	95.26 ± 0.21	21.96

Table 6: Effect of patch size on classification performance for the **OCTMNIST** dataset. Acc.: Accuracy, Bal. Acc.: Balanced Accuracy, AUC: Area under the ROC curve, GFLOPs: Giga Floating-Point Operations.

Patch size	Acc. (%)	Bal. Acc. (%)	AUC (%)	GFLOPs
1	76.60 ± 2.10	76.60 ± 2.10	95.66 ± 0.28	16.71
2	79.10 ± 0.85	79.10 ± 0.85	96.68 ± 0.39	4.19
4	78.63 ± 1.26	78.63 ± 1.26	96.25 ± 0.23	1.06
7	78.03 ± 0.15	78.03 ± 0.15	95.62 ± 0.05	0.36
14	71.70 ± 0.66	71.70 ± 0.66	93.02 ± 0.41	0.11
28	67.37 ± 0.06	67.37 ± 0.06	91.24 ± 0.07	0.04
(1, 2, 4)	79.90 ± 0.67	79.90 ± 0.67	97.18 ± 0.11	21.96

Table 7: Effect of patch size on classification performance for the **OrganMNIST** dataset. Acc.: Accuracy, Bal. Acc.: Balanced Accuracy, AUC: Area under the ROC curve, GFLOPs: Giga Floating-Point Operations.

Patch size	Acc. (%)	Bal. Acc. (%)	AUC (%)	GFLOPs
1	78.63 \pm 0.23	74.96 \pm 0.57	97.65 \pm 0.07	16.71
2	80.54 \pm 0.29	76.51 \pm 0.10	98.08 \pm 0.11	4.19
4	80.50 \pm 0.37	76.35 \pm 0.57	97.98 \pm 0.11	1.06
7	79.06 \pm 0.80	74.42 \pm 0.95	97.71 \pm 0.14	0.36
14	74.82 \pm 1.25	70.71 \pm 1.29	96.95 \pm 0.33	0.11
28	68.42 \pm 0.77	63.73 \pm 1.25	95.29 \pm 0.09	0.04
(1, 2, 4)	82.79 \pm 0.33	78.77 \pm 0.44	98.38 \pm 0.03	21.96

Table 8: Effect of patch size on classification performance for the **PneumoniaMNIST** dataset. Acc.: Accuracy, Bal. Acc.: Balanced Accuracy, AUC: Area under the ROC curve, GFLOPs: Giga Floating-Point Operations).

Patch size	Acc. (%)	Bal. Acc. (%)	AUC (%)	GFLOPs
1	90.28 \pm 0.67	87.27 \pm 0.84	98.53 \pm 0.55	16.71
2	91.93 \pm 1.53	89.62 \pm 2.12	98.70 \pm 0.07	4.19
4	90.33 \pm 0.34	87.45 \pm 0.45	98.55 \pm 0.08	1.06
7	89.47 \pm 0.49	86.25 \pm 0.86	97.91 \pm 0.09	0.36
14	90.38 \pm 1.00	87.66 \pm 1.51	97.66 \pm 0.21	0.11
28	89.10 \pm 0.73	85.84 \pm 1.01	97.49 \pm 0.20	0.04
(1, 2, 4)	91.61 \pm 0.30	89.07 \pm 0.41	98.71 \pm 0.14	21.96

3.3. 3D Datasets

Across the 3D datasets (AdrenalMNIST3D, FractureMNIST3D, NoduleMNIST3D, SynapseMNIST3D, and VesselMNIST3D), the results in Tables 9–13 show a trend regarding the effect of patch size on ViT performance. Similar to the 2D experiments, smaller volumetric patches generally lead to better classification results. Patch size 1 achieves the best or second-best performance across most datasets in terms of Acc., Bal. Acc., and AUC. As the patch size increases, we observe a decrease in classification performance. For 3D datasets, larger patch sizes deliver inferior results, with patch sizes 14 and 28 yielding the worst overall performance. The performances with these two patch sizes are very similar (average Acc., Bal. Acc., and AUC of 73.61%, 55.73% , and 69.99% for patch size 14 versus 73.38%, 56.40%, and 70.86% for patch size 28), with patch size 14 performing slightly worse overall. In comparison, the best overall performance is achieved with patch size 1, with average Acc., Bal. Acc., and AUC of 77.09%, 66.96%, and 80.83%. Both larger patch sizes therefore, deliver inferior results by a large margin.

A detailed comparison between patch size 1 and patch size 14 is provided in Table S2 in the supplementary material. The largest gain in Acc. is observed in the FractureMNIST3D dataset, with a 10% improvement. The largest gains in Bal. Acc. and AUC are seen in the VesselMNIST3D dataset, with improvements of 23.78% and 19.37%, respectively.

Additionally, it can be observed that the proposed fusion approach (prediction fusion of models trained with patch sizes 1, 2, and 4) provides improved performance for some datasets, although its effect is less pronounced compared with the 2D experiments.

3.4. Merged Results

Overall, our experimental results show improved classification performance when ViT models are fine-tuned with smaller patch sizes for both 2D and 3D datasets. However, this performance gain comes at the cost of increased computational complexity, as reflected in the GFLOPs reported in all tables. For the 2D datasets, reducing the patch size from 28 to 1 improves accuracy but raises the computational cost from 0.04 GFLOPs to 16.71 GFLOPs per image. For the 3D datasets, the effect is even more pronounced. Decreasing the patch size from 28 to 1 increases the computational cost from approximately 0.40 GFLOPs to more than 800 GFLOPs per volume. Although the computational cost increases with smaller patch sizes, it is important to note that this increase is not solely due to the overhead of

Table 9: Effect of patch size on classification performance for the **AdrenalMNIST3D** dataset. Acc.: Accuracy, Bal. Acc.: Balanced Accuracy, AUC: Area under the ROC curve, GFLOPs: Giga Floating-Point Operations.

Patch size	Acc. (%)	Bal. Acc. (%)	AUC (%)	GFLOPs
1	80.20 ± 2.51	68.72 ± 3.61	82.56 ± 2.89	800.85
2	81.88 ± 0.72	65.76 ± 1.15	79.16 ± 1.47	117.83
4	78.64 ± 0.63	61.12 ± 2.28	73.92 ± 1.59	19.90
7	76.29 ± 0.88	57.74 ± 1.23	76.47 ± 2.28	3.10
14	77.29 ± 1.61	60.59 ± 3.42	78.58 ± 1.97	0.57
28	76.96 ± 1.04	58.68 ± 1.53	78.76 ± 1.28	0.40
(1, 2, 4)	81.54 ± 0.82	64.70 ± 0.89	83.38 ± 1.14	938.58

Table 10: Effect of patch size on classification performance for the **FractureMNIST3D** dataset. Acc.: Accuracy, Bal. Acc.: Balanced Accuracy, AUC: Area under the ROC curve, GFLOPs: Giga Floating-Point Operations.

Patch size	Acc. (%)	Bal. Acc. (%)	AUC (%)	GFLOPs
1	56.11 ± 2.21	52.56 ± 5.22	73.79 ± 2.13	816.97
2	53.33 ± 1.80	49.51 ± 2.45	69.23 ± 2.33	120.2
4	55.97 ± 3.07	47.79 ± 2.99	68.78 ± 0.61	20.3
7	49.86 ± 1.61	44.51 ± 2.67	64.57 ± 1.44	3.16
14	46.11 ± 2.73	40.05 ± 1.54	61.42 ± 1.61	0.58
28	47.22 ± 1.53	42.34 ± 0.95	62.25 ± 0.42	0.41
(1, 2, 4)	57.78 ± 1.87	51.48 ± 1.74	74.86 ± 1.55	957.47

Table 11: Effect of patch size on classification performance for the **NoduleMNIST3D** dataset. Acc.: Accuracy, Bal. Acc.: Balanced Accuracy, AUC: Area under the ROC curve, GFLOPs: Giga Floating-Point Operations.

Patch size	Acc. (%)	Bal. Acc. (%)	AUC (%)	GFLOPs
1	85.38 ± 1.06	76.91 ± 2.58	89.41 ± 0.39	811.74
2	84.84 ± 0.70	78.50 ± 0.54	88.79 ± 1.61	119.43
4	84.84 ± 0.70	75.23 ± 0.42	85.75 ± 0.87	20.17
7	83.87 ± 0.95	72.69 ± 0.82	84.84 ± 0.35	3.14
14	83.87 ± 0.70	72.11 ± 1.58	82.06 ± 0.90	0.57
28	84.73 ± 0.40	72.85 ± 2.37	81.49 ± 1.32	0.40
(1, 2, 4)	85.59 ± 0.40	76.86 ± 0.41	89.16 ± 0.45	951.34

Table 12: Effect of patch size on classification performance for the **SynapseMNIST3D** dataset. Acc.: Accuracy, Bal. Acc.: Balanced Accuracy, AUC: Area under the ROC curve, GFLOPs: Giga Floating-Point Operations.

Patch size	Acc. (%)	Bal. Acc. (%)	AUC (%)	GFLOPs
1	71.02 ± 0.70	56.93 ± 1.84	64.12 ± 1.27	816.97
2	70.74 ± 1.62	53.42 ± 2.32	58.76 ± 2.43	120.20
4	72.73 ± 0.40	50.80 ± 0.65	56.72 ± 4.38	20.30
7	73.58 ± 0.80	51.05 ± 1.49	57.60 ± 2.04	3.16
14	73.01 ± 0.00	50.00 ± 0.00	52.98 ± 0.51	0.58
28	69.70 ± 1.14	50.27 ± 1.05	57.22 ± 0.24	0.41
(1, 2, 4)	72.73 ± 0.61	52.02 ± 1.29	63.99 ± 1.4	957.47

Table 13: Effect of patch size on classification performance for the **VesselMNIST3D** dataset. Acc.: Accuracy, Bal. Acc.: Balanced Accuracy, AUC: Area under the ROC curve, GFLOPs: Giga Floating-Point Operations.

Patch size	Acc. (%)	Bal. Acc. (%)	AUC (%)	GFLOPs
1	92.76 ± 0.33	79.67 ± 1.41	94.28 ± 1.48	812.72
2	91.19 ± 0.65	72.70 ± 5.38	90.74 ± 1.05	119.57
4	90.49 ± 1.23	70.95 ± 5.23	87.49 ± 2.96	20.19
7	88.05 ± 1.58	57.05 ± 1.92	73.89 ± 1.55	3.14
14	87.78 ± 0.49	55.89 ± 3.09	74.91 ± 0.32	0.57
28	88.31 ± 0.99	57.88 ± 5.05	74.59 ± 0.82	0.40
(1, 2, 4)	92.84 ± 0.33	73.29 ± 1.01	94.13 ± 0.52	952.48

self-attention. Other components such as the classification head, patch embedding, and various constant or linear terms also contribute to the FLOPs. In summary, for the 2D datasets we observed that the GFLOPs increase by a factor of about four when the patch size is halved, while for the 3D datasets the increase is typically around a factor of five to seven. The one exception occurs at larger patch sizes for 3D datasets, particularly between patch sizes 14 and 28, where very few tokens remain and constant overheads begin to dominate the total computational cost.

Besides the main results reported in the tables, we also provide the confusion matrices for the best-performing models (fine-tuned with patch sizes 1, 2, and 4, as well as the ensemble) for all 12 datasets in Figure S1, Figure S2, Figure S3, and Figure S4 in the supplementary material.

For a visual comparison between patch size 2 and patch size 28, we extracted attention maps from the final transformer layer for some sample images. We selected ViTs with patch sizes 2 (P2) and 28 (P28), representing the overall best and worst performing configurations. We then identified samples that were misclassified by the P28 model but correctly classified by the P2 model and present the corresponding attention heatmaps for representative examples in Figure 4. As observed, models using smaller patch sizes (P2) exhibit more focused and detailed attention on diagnostically relevant regions. In contrast, models with larger patches of 28 show uniform attention patterns. This suggests that localized attention contributes to improved feature extraction for classification task.

For better comparison, we also provide bar charts for all datasets based on the three evaluation metrics in Figure 5. As expected, smaller patches and their ensembles generally yield the best results. We additionally present the average performance in relation to patch size across all 2D datasets, all 3D datasets, and all datasets combined in Figure 6. As illustrated, there is a clear upward trend as patch sizes decrease.

Despite providing an in-depth analysis of patch-size effects in ViTs for medical image classification, this study has some limitations. First, all experiments were conducted on a single GPU, which limited the choice of model capacity. As a result, we only analyzed the ViT-Small architecture. Larger models such as ViT-Large or ViT-Huge could also be considered in future analyses and might benefit even more from detailed tokenization. However, running these models would require substantially more GPU memory and computing power, which was outside the scope of this work.

Second, although we demonstrated clear benefits from using smaller patch

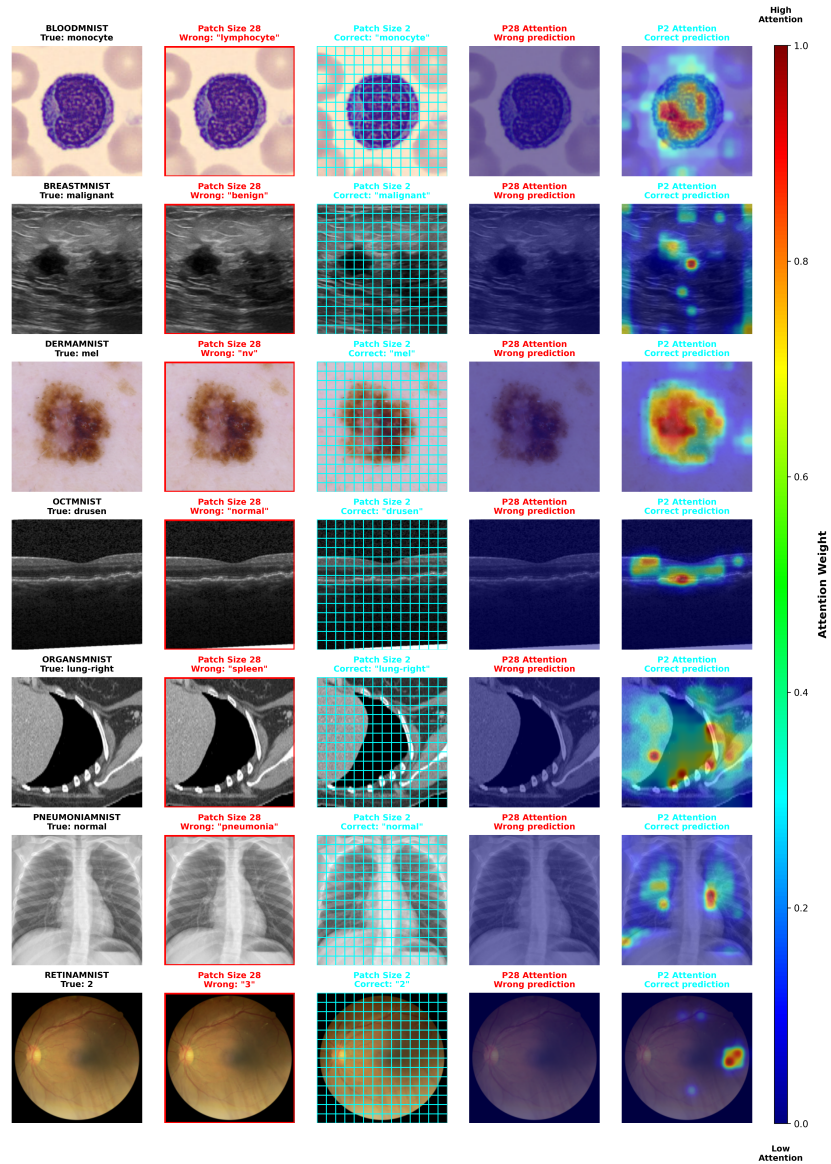


Figure 4: Comparison of attention maps for patch sizes of 2 and 28 for some example images. The figure shows original images with patch grids (left three columns) and corresponding attention heatmaps (right two columns). Models with smaller patch sizes (P2) consistently achieve correct predictions with more focused attention patterns, while larger patch sizes (P28) lead to incorrect predictions with less informative attention distributions.

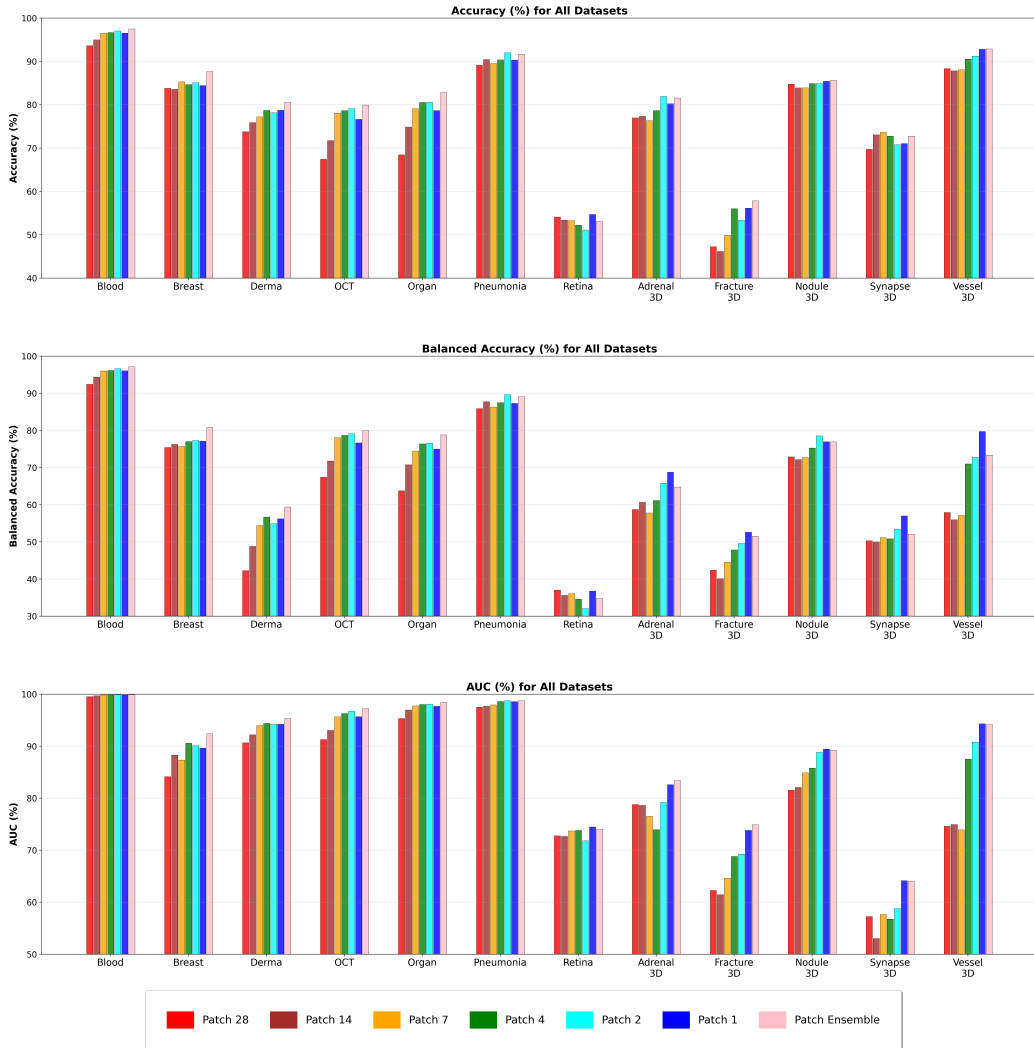


Figure 5: Effect of patch size on vision transformer classification performance across 12 medical image datasets (seven 2D and five 3D datasets from the MedMNIST V2 collection)

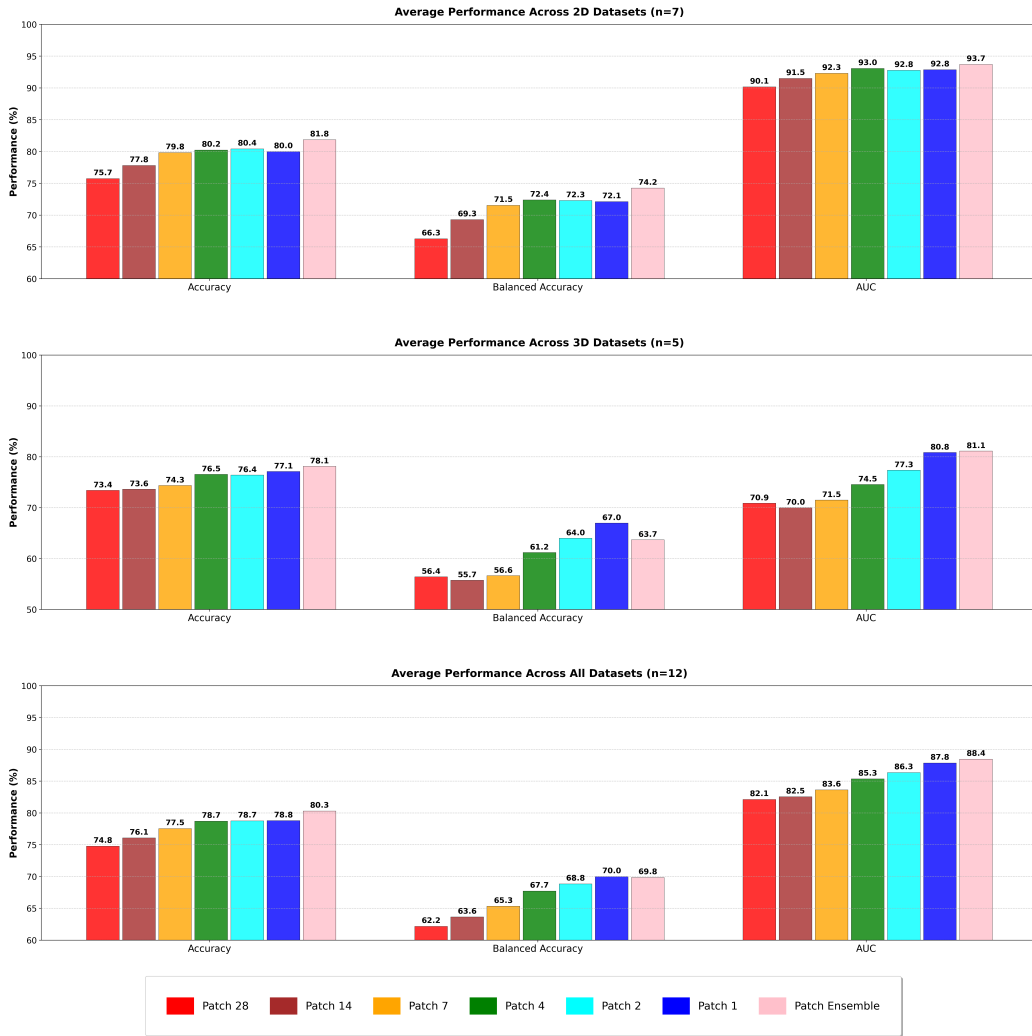


Figure 6: Effect of patch size on vision transformer performance: average across different dataset groups

sizes, this improvement comes with significant computational costs, especially for 3D datasets. This poses challenges for deploying such models in real-world clinical settings, particularly in hospitals with limited hardware resources or scenarios requiring real-time processing.

Finally, our experiments were based on MedMNIST v2. While this allowed for a systematic comparison across many datasets from different medical imaging modalities, these datasets may not fully reflect the resolution and complexity of real clinical images. Future work should investigate whether the patch-size trends observed here also hold for real-world high-resolution clinical datasets.

4. Conclusion

In this work, we present the first thorough investigation of how patch size affects ViT classification performance in both 2D and 3D medical imaging. Using 12 datasets from the MedMNIST v2 collection, our overall results show that using smaller patch sizes leads to improved performance for both 2D and 3D datasets. This trend is particularly more evident for medium- to large-scale 2D datasets and for all 3D datasets, indicating that finer tokenization enables ViTs to capture more localized and clinically relevant features.

However, these performance gains come with substantial computational costs, as attention complexity grows rapidly with the number of tokens. This challenge is especially pronounced for 3D ViTs, where volumetric patching results in significantly larger token counts. Nevertheless, our experiments demonstrate that such analyses are still feasible on a single GPU when appropriately small image sizes are used, highlighting that patch-size studies can be performed without large-scale computational infrastructure.

Overall, our findings reveal a clear connection between patch size and model performance, providing practical guidance for designing ViT-based pipelines in medical image analysis.

Declaration of Competing Interest

The authors declare that they have no known competing financial interests that could have appeared to influence the work reported in this paper.

Data Availability

The datasets used in this study are publicly available from previously published papers. The code developed for this study is available on GitHub, with the corresponding link provided in the manuscript.

Ethics Statement

Ethical approval was not required for this study, as all datasets used are publicly available and were previously published [37].

CRedit Authorship Contribution Statement

Massoud Dehghan: Conceptualization, Methodology, Writing – original draft, Writing – review and editing, Formal analysis, Software, Validation. **Ramona Woitek:** Supervision, Validation, Writing – review and editing, Project administration. **Amirreza Mahbod:** Supervision, Conceptualization, Methodology, Writing – original draft, Writing – review and editing, Formal analysis, Software, Validation, Project administration.

Declaration of generative AI and AI-assisted technologies in the manuscript preparation process

During the preparation of this work, the authors used ChatGPT (version 5.1) to check grammar and spelling and, at times, improve the readability of some sentences. After using these tools, the authors reviewed and edited the content as needed and take full responsibility for the content of the publication.

References

- [1] Mengfang Li, Yuanyuan Jiang, Yanzhou Zhang, and Haisheng Zhu. Medical image analysis using deep learning algorithms. *Frontiers in Public Health*, Volume 11 - 2023, 2023.
- [2] Palak Handa, Manas Dhir, Amirreza Mahbod, Florian Schwarzhans, Ramona Woitek, Nidhi Goel, and Deepak Gunjan. Wcebleedgen: A wireless capsule endoscopy dataset and its benchmarking for automatic bleeding classification, detection, and segmentation. *arXiv preprint arXiv:2408.12466*, 2024.

- [3] Muhammad Razzak, Saeeda Naz, and Ahmad Zaib. *Deep Learning for Medical Image Processing: Overview, Challenges and the Future*, pages 323–350. 2018.
- [4] Andre Esteva, Alexandre Robicquet, Bharath Ramsundar, Volodymyr Kuleshov, Mark DePristo, Katherine Chou, Claire Cui, Greg Corrado, Sebastian Thrun, and Jeff Dean. A guide to deep learning in healthcare. *Nature Medicine*, 25, 2019.
- [5] Fabio A. Spanhol, Luiz S. Oliveira, Caroline Petitjean, and Laurent Heutte. A dataset for breast cancer histopathological image classification. *IEEE Transactions on Biomedical Engineering*, 63(7):1455–1462, 2016.
- [6] Kaiming He, Xiangyu Zhang, Shaoqing Ren, and Jian Sun. Deep residual learning for image recognition. In *IEEE Conference on Computer Vision and Pattern Recognition*, pages 770–778, 2016.
- [7] Gao Huang, Zhuang Liu, Laurens Van Der Maaten, and Kilian Q. Weinberger. Densely connected convolutional networks. In *IEEE Conference on Computer Vision and Pattern Recognition*, pages 2261–2269, 2017.
- [8] Mingxing Tan and Quoc Le. EfficientNet: Rethinking model scaling for convolutional neural networks. In Kamalika Chaudhuri and Ruslan Salakhutdinov, editors, *Proceedings of the 36th International Conference on Machine Learning*, volume 97 of *Proceedings of Machine Learning Research*, pages 6105–6114. PMLR, 2019.
- [9] Mingxing Tan and Quoc Le. EfficientNetV2: Smaller models and faster training. In Marina Meila and Tong Zhang, editors, *Proceedings of the 38th International Conference on Machine Learning*, volume 139 of *Proceedings of Machine Learning Research*, pages 10096–10106. PMLR, 2021.
- [10] Amirreza Mahbod, Gerald Schaefer, Rupert Ecker, and Isabella Ellinger. Pollen grain microscopic image classification using an ensemble of fine-tuned deep convolutional neural networks. In *International Conference on Pattern Recognition*, pages 344–356. Springer, 2021.
- [11] Alex Krizhevsky, Ilya Sutskever, and Geoffrey E Hinton. Imagenet classification with deep convolutional neural networks. In F. Pereira, C.J.

- Burges, L. Bottou, and K.Q. Weinberger, editors, *Advances in Neural Information Processing Systems*, volume 25. Curran Associates, Inc., 2012.
- [12] Gao Huang, Zhuang Liu, Laurens Van Der Maaten, and Kilian Q. Weinberger. Densely connected convolutional networks. In *2017 IEEE Conference on Computer Vision and Pattern Recognition (CVPR)*, pages 2261–2269, 2017.
- [13] Mingxing Tan and Quoc Le. EfficientNet: Rethinking model scaling for convolutional neural networks. In Kamalika Chaudhuri and Ruslan Salakhutdinov, editors, *Proceedings of the 36th International Conference on Machine Learning*, volume 97 of *Proceedings of Machine Learning Research*, pages 6105–6114. PMLR, 2019.
- [14] Dinggang Shen, Guorong Wu, and Heung-Il Suk. Deep learning in medical image analysis. *Annual Review of Biomedical Engineering*, 19(Volume 19, 2017):221–248, 2017.
- [15] Alexey Dosovitskiy, Lucas Beyer, Alexander Kolesnikov, Dirk Weissenborn, Xiaohua Zhai, Thomas Unterthiner, Mostafa Dehghani, Matthias Minderer, Georg Heigold, Sylvain Gelly, Jakob Uszkoreit, and Neil Houlsby. An image is worth 16x16 words: Transformers for image recognition at scale. *arXiv preprint arXiv:2010.11929*, 2020.
- [16] Ashish Vaswani, Noam Shazeer, Niki Parmar, Jakob Uszkoreit, Llion Jones, Aidan N Gomez, Łukasz Kaiser, and Illia Polosukhin. Attention is all you need. In I. Guyon, U. Von Luxburg, S. Bengio, H. Wallach, R. Fergus, S. Vishwanathan, and R. Garnett, editors, *Advances in Neural Information Processing Systems*, volume 30. Curran Associates, Inc., 2017.
- [17] Reza Azad, Amirhossein Kazerouni, Moein Heidari, Ehsan Khodapanah Aghdam, Amirali Molaei, Yiwei Jia, Abin Jose, Rijo Roy, and Dorit Merhof. Advances in medical image analysis with vision transformers: A comprehensive review. *Medical Image Analysis*, 91:103000, 2024.
- [18] Ashish Vaswani, Noam Shazeer, Niki Parmar, Jakob Uszkoreit, Llion Jones, Aidan N. Gomez, Łukasz Kaiser, and Illia Polosukhin. Attention is all you need. In *Proceedings of the 31st International Conference on*

Neural Information Processing Systems, NIPS'17, page 6000–6010, Red Hook, NY, USA, 2017. Curran Associates Inc.

- [19] Yin Dai, Yifan Gao, and Fayu Liu. Transmed: Transformers advance multi-modal medical image classification. *Diagnostics*, 11, 2021.
- [20] Sanad Aburass, Osama Dorgham, Jamil Al Shaqsi, Maha Abu Ruman, and Omar Al-Kadi. Vision transformers in medical imaging: a comprehensive review of advancements and applications across multiple diseases. *Journal of imaging informatics in medicine*, 2025.
- [21] Satoshi Takahashi, Yusuke Sakaguchi, Nobuji Kouno, Ken Takasawa, Kenichi Ishizu, Yu Akagi, Rina Aoyama, Naoki Teraya, Amina Bolatkan, Norio Shinkai, Hidenori Machino, Kazuma Kobayashi, Ken Asada, Masaaki Komatsu, Syuzo Kaneko, Masashi Sugiyama, and Ryuji Hamamoto. Comparison of vision transformers and convolutional neural networks in medical image analysis: A systematic review. *Journal of Medical Systems*, 48(1):84, Sep 2024.
- [22] Zifeng Wang, Zhenbang Wu, Dinesh Agarwal, and Jimeng Sun. Med-CLIP: Contrastive learning from unpaired medical images and text. *arXiv preprint arXiv:2210.10163*, 2022.
- [23] Sheng Zhang, Yanbo Xu, Naoto Usuyama, Hanwen Xu, Jaspreet Bagga, Robert Tinn, Sam Preston, Rajesh Rao, Mu Wei, Naveen Valluri, et al. BiomedCLIP: a multimodal biomedical foundation model pre-trained from fifteen million scientific image-text pairs. *arXiv preprint arXiv:2303.00915*, 2023.
- [24] Richard J. Chen, Tong Ding, Ming Y. Lu, Drew F. K. Williamson, Guillaume Jaume, Andrew H. Song, Bowen Chen, Andrew Zhang, Daniel Shao, Muhammad Shaban, Mane Williams, Lukas Oldenburg, Luca L. Weishaupt, Judy J. Wang, Anurag Vaidya, Long Phi Le, Georg Gerber, Sharifa Sahai, Walt Williams, and Faisal Mahmood. Towards a general-purpose foundation model for computational pathology. *Nature Medicine*, 30(3):850–862, 2024.
- [25] Gabriel Ilharco, Mitchell Wortsman, Ross Wightman, Cade Gordon, Nicholas Carlini, Rohan Taori, Achal Dave, Vaishaal Shankar, Hongseok

- Namkoong, John Miller, Hannaneh Hajishirzi, Ali Farhadi, and Ludwig Schmidt. Openclip, 2021.
- [26] Amirreza Mahbod, Nematollah Saeidi, Sepideh Hatamikia, and Ramona Woitek. Evaluating pre-trained convolutional neural networks and foundation models as feature extractors for content-based medical image retrieval. *Engineering Applications of Artificial Intelligence*, 150:110571, 2025.
- [27] Nematollah Saeidi, Hossein Karshenas, Bijan Shoushtarian, Sepideh Hatamikia, Ramona Woitek, and Amirreza Mahbod. Leveraging medical foundation model features in graph neural network-based retrieval of breast histopathology images. *arXiv preprint arXiv:2405.04211*, 2024.
- [28] Nematollah Saeidi, Nima Torbati, Ramona Woitek, and Amirreza Mahbod. Integrating foundation model features into graph neural network and fusing predictions with standard fine-tuned models for histology image classification. *Bioengineering*, 12(12), 2025.
- [29] Ze Liu, Yutong Lin, Yue Cao, Han Hu, Yixuan Wei, Zheng Zhang, Stephen Lin, and Baining Guo. Swin transformer: Hierarchical vision transformer using shifted windows. In *Proceedings of the IEEE/CVF International Conference on Computer Vision (ICCV)*, pages 10012–10022, 2021.
- [30] Ze Liu, Han Hu, Yutong Lin, Zhuliang Yao, Zhenda Xie, Yixuan Wei, Jia Ning, Yue Cao, Zheng Zhang, Li Dong, Furu Wei, and Baining Guo. Swin transformer v2: Scaling up capacity and resolution. In *2022 IEEE/CVF Conference on Computer Vision and Pattern Recognition (CVPR)*, pages 11999–12009, 2022.
- [31] Stéphane D’Ascoli, Hugo Touvron, Matthew L Leavitt, Ari S Morcos, Giulio Biroli, and Levent Sagun. Convit: Improving vision transformers with soft convolutional inductive biases. In Marina Meila and Tong Zhang, editors, *Proceedings of the 38th International Conference on Machine Learning*, volume 139 of *Proceedings of Machine Learning Research*, pages 2286–2296. PMLR, 2021.
- [32] Zihang Dai, Hanxiao Liu, Quoc V Le, and Mingxing Tan. Coatnet: Marrying convolution and attention for all data sizes. In M. Ranzato,

- A. Beygelzimer, Y. Dauphin, P.S. Liang, and J. Wortman Vaughan, editors, *Advances in Neural Information Processing Systems*, volume 34, pages 3965–3977. Curran Associates, Inc., 2021.
- [33] Nima Torbati, Anastasia Meshcheryakova, Ramona Woitek, Diana Mechtcheriakova, and Amirreza Mahbod. Acs-segnet: An attention-based cnn-segformer segmentation network for tissue segmentation in histopathology. *arXiv preprint arXiv:2510.20754*, 2025.
- [34] Joel C. M. Than, Pun Liang Thon, Omar Mohd Rijal, Rosminah M. Kassim, Ashari Yunus, Norliza M. Noor, and Patrick Then. Preliminary study on patch sizes in vision transformers (vit) for covid-19 and diseased lungs classification. In *2021 IEEE National Biomedical Engineering Conference (NBEC)*, pages 146–150, 2021.
- [35] Yue Liu, Christos Matsoukas, Fredrik Strand, Hossein Azizpour, and Kevin Smith. Patchdropout: Economizing vision transformers using patch dropout. In *IEEE/CVF Winter Conference on Applications of Computer Vision*, pages 3942–3951, 2023.
- [36] A. Halder, S. Gharami, P. Sadhu, et al. Implementing vision transformer for classifying 2d biomedical images. *Scientific Reports*, 14:12567, 2024.
- [37] Jiancheng Yang, Rui Shi, Donglai Wei, Zequan Liu, Lin Zhao, Bilian Ke, Hanspeter Pfister, and Bingbing Ni. MedMNIST v2 - a large-scale lightweight benchmark for 2d and 3d biomedical image classification. *Scientific Data*, 10(1):41, 2023.
- [38] Lucas Beyer, Pavel Izmailov, Alexander Kolesnikov, Mathilde Caron, Simon Kornblith, Xiaohua Zhai, Matthias Minderer, Michael Tschannen, Ibrahim Alabdulmohsin, and Filip Pavetic. Flexivit: One model for all patch sizes. In *2023 IEEE/CVF Conference on Computer Vision and Pattern Recognition (CVPR)*, pages 14496–14506, 2023.
- [39] Duy-Kien Nguyen, Mahmoud Assran, Unnat Jain, Martin R. Oswald, Cees G Snoek, and Xinlei Chen. An image is worth more than 16x16 patches: Exploring transformers on individual pixels. In Y. Yue, A. Garg, N. Peng, F. Sha, and R. Yu, editors, *International Conference on Representation Learning*, volume 2025, pages 59753–59773, 2025.

- [40] Feng Wang, Yaodong Yu, Guoyizhe Wei, Wei Shao, Yuyin Zhou, Alan Yuille, and Cihang Xie. Scaling laws in patchification: An image is worth 50,176 tokens and more. 2025.
- [41] Cagla Deniz Bahadir, Mohamed Omar, Jacob Rosenthal, Luigi Marchionni, Benjamin Liechty, David J. Pisapia, and Mert R. Sabuncu. Artificial intelligence applications in histopathology. *Nature Reviews Electrical Engineering*, 1(2):93–108, Feb 2024.
- [42] Xiaohua Zhai, Alexander Kolesnikov, Neil Houlsby, and Lucas Beyer. Scaling vision transformers. In *Proceedings of the IEEE/CVF Conference on Computer Vision and Pattern Recognition (CVPR)*, pages 12104–12113, 2022.
- [43] Feyza Duman Keles, Pruthuvi Mahesakya Wijewardena, and Chinmay Hegde. On the computational complexity of self-attention. In Shipra Agrawal and Francesco Orabona, editors, *Proceedings of The 34th International Conference on Algorithmic Learning Theory*, volume 201 of *Proceedings of Machine Learning Research*, pages 597–619. PMLR, 2023.
- [44] Jia Deng, Wei Dong, Richard Socher, Li-Jia Li, Kai Li, and Li Fei-Fei. Imagenet: A large-scale hierarchical image database. In *IEEE Conference on Computer Vision and Pattern Recognition*, pages 248–255, 2009.
- [45] João Carreira and Andrew Zisserman. Quo vadis, action recognition? a new model and the kinetics dataset. In *IEEE Conference on Computer Vision and Pattern Recognition*, pages 4724–4733, 2017.
- [46] Ilya Loshchilov and Frank Hutter. Decoupled weight decay regularization. *arXiv preprint arXiv:1711.05101*, 2017.